Proceedings of the World Congress on New Technologies (NewTech 2015)
Barcelona, Spain – July 15 - 17, 2015
Paper No. 307

Developing Cost Effective Graphene Conductive Coating and its Application as Counter Electrode for CdS Quantum Dot Sensitized Solar Cell

Amr Hessein, Ahmed Abd El-Moneim
Material Science and Engineering Department MSE,
Egypt-Japan University of Science and Technology (E-JUST),
New Borg El Arab, Alexandria, Egypt.
amr.ahmed@ejust.edu.eg ; ahmed.abdelmoneim@ejust.edu.eg

Abstract **-**A low cost, chemically stable with enhanced electrocatalytic activity counter electrodes based on reduced graphene oxide (RGO) coating was easily deposited on fluorine doped tin oxide (FTO) substrate was developed for CdS QDSSCs. Polyvinylidene fluoride (PVDF) was used as a binder for the coating to increase the mechanical stability of RGO counter electrode through increasing its adhesion on the FTO substrate. The structure and morphology of RGO powder were analysed by UV-visible, FTIR spectroscopy, X-ray powder diffraction, and SEM microscopy. The electrocatalytic activity of RGO counter electrodes were investigated by cyclic voltammetry (CV) and electrochemical impedance spectroscopy (EIS). The QDSSCs assembled using RGO counter electrode shows a high short circuit current reaches to a value of 2.843 mA\ cm^2 and yields power conversion efficiency (PCE) of 0.52%. An enhancement 46.3% in the fill factor (FF) also was achieved with RGO as a counter electrode when compared to expensive traditional Pt thin film counter electrode. The unique electrocatalytic activity of the tailored RGO electrode was discussed in terms of its high electrical conductivity and large surface area.

Keywords**:** QDSSCs, RGO, Counter electrode, Polysulfide electrolyte.

1. Introduction

Among the newly developed materials nanostructures, Graphene got a lot of scientists' attention as the next generation nanomaterials due to its low production cost, abundance of carbon on earth, and its exceptional unique properties (Choi et al. 2010). Graphene is a 2- dimensional planer sheet of sp^2-hybridized bonded carbon atoms densely packed in a honeycomb crystal lattice with single atom thickness (Geim and Novoselov 2007). With large surface area, 0 eV bandgap, excellent electrical conductivity, and high intrinsic electron mobility, graphene became the strongest candidate to replace the others carbonaceous materials in electronics, electrochemical, and photo- electrochemical applications (Kucinskis, Bajars, and Kleperis 2013; Li et al. 2012; Strong et al. 2012). The problem of mass production was the large obstacle that facing the developing of scalable commercial devices based on graphene. Graphene that prepared by direct mechanical exfoliation from pristine graphite or that prepared by chemical vapour deposition is produced in small quantities and not suitable for low cost and large scale production, but it can used only for scientific research (Pei and Cheng 2012). Producing graphene from exfoliation graphite oxide and reduction of graphene oxide (GO) can produce larger quantities of graphene which can be applicable on the industrial scale (Gamil et al. 2014). It is already known that the morphological and electrical properties of reduced graphene oxide (RGO) are lower when compared to the pristine graphene, but RGO obviously enhances the performance of all applications when it replaces the others carbonaceous materials (Hassan, Suzuki, and El-moneim 2014).

Quantum dot sensitized solar cell (QDSSC) that belongs to the third generation solar cell is a promising candidate to replace the widespread wafer based solar cell from the first generation (Kouhnavard et al. 2014). QDSSC is a modified version of dye sensitized solar cell (DSSC) that invented in 1991 by Grätzel and O Regan (O'Regan and Grätzel 1991). The dye molecules adsorbed on wide bandgap semiconductor mesoporous film in DSSC is replaced with narrow bandgap semiconductor nanoparticles (Kamat 2008). The ease of fabrication, the low cost, and the high

theoretical power conversion efficiency (PCE) were the reasons made the scientists to intensively investigating and developing nanostructured material for enhancing the performance of QDSSCs (Badawi et al. 2013). semiconductor nanoparticles (QDs) offer a number of unique properties over the complex dyes used in DSSCs such as tunability of the bandgap, large intrinsic dipole moment, high molar absorption coefficient, and multiple carrier generation by a single photon (Kouhnavard et al. 2014; Rühle, Shalom, and Zaban 2010). These unique properties are theoretically aimed to raise the PCE beyond the Shockley and Queisser limit of 32%. Until now the PCE of QDSSCs are still lower the PCE of DSSCs and far away from the theoretical calculated values. The high recombination rate at the active layer- electrolyte interface, the lack for the suitable redox system, and the scarcity of perfect counter electrode are the main reasons for inefficient utilization of the photogenerated electrons in QDSSCs.

In this work, we develop a feasible low cost, chemically stable, and reproducible electrically conducting coating based on RGO and used as counter electrode for QDSSCs. A thin film from the RGO coating was produced on fluorine doped tin oxide (FTO) substrate by simple drop casting method. RGO counter electrodes showed better electrocatalytic activity towards the reduction of polysulfide electrolyte ($S^{2-}\backslash S_x^{2-}$) than the expensive and widely used platinum (Pt) counter electrode. CdS QDSSCs that employed RGO counter electrodes showed better photovoltaic performance than that use Pt counter electrode. The high PCE and FF obtained in the cells with RGO counter electrode was a result of the high electric conductivity and the good catalytic activity of the RGO towards the polysulfide electrolyte as well as its large surface area which promotes more active sites for better regeneration process of the ($S^{2-}\backslash S_x^{2-}$) electrolyte.

2. Experimental Work

2. 1. RGO Counter Electrode Preparation

Graphite oxide was prepared according to Hummer and Offeman's method with some modification as reported elsewhere (Becerril et al. 2008a, 2008b; Sui et al. 2011). Graphite oxide was dispersed in distilled water at concentration of 1 mg/ml using magnetic stirrer. Graphite oxide was exfoliated into Graphene oxide (GO) by ultrasonication for 30 min in ultrasonic bath (Falcon RS2). GO sheets was chemically reduced into Graphene with using Hydrazine hydrate as a reducing agent and continuous heating at ~80 ^{o}C overnight. The chemically reduced graphene (RGO) powder was separated and washed with distilled water via vacuum filtration and dried to get yield the RGO powder. RGO conducting coating was made by mixing 50 mg of prepared RGO powder with 5 mg PVDF (10% w/w) and then dispersed in 3 ml N-Methyl pyrrolidinone (NMP) through ultrasonication for 60 min. The PVDF polymer was used to prevent re-stacking of graphene sheets in the paste as well as a binder to increase the adhesion of RGO on FTO substrate. The RGO thin film counter electrode was prepared by drop casting 50 µl of RGO dispersion on pre-cleaned FTO slide of exposed area 1 cm^2 followed by drying at moderate temperature and under vacuum for 24 hours to form the counter electrode.

2. 2. Tio_2 Photoanode Preparation

The photoanode is prepared on FTO coated glass (Pilkington TEC15, surface resistivity ~13 Ω/sq) that was first ultrasonically cleaned using detergent solution, water, and acetone respectively. A dense TiO_2 blocking layer was first formed on the FTO by spin coating 0.1 M Titanium Isopropoxide (TIP) in isopropanol at 1000 rpm for 10 seconds, followed by sintering at 500 ^{o}C for 1 hour (Barceló et al. 2012). A mesoporous TiO_2 layer was formed over the blocking layer by coating TiO_2 aqueous paste using doctor blade technique followed by sintering at 500 ^{o}C for 1 hour. The TiO_2 prepared by grinding 1 g of TiO_2 powder with1.8 mL of H_2O, 30 µL of acetylacetone, and 30 µL of Triton X-100 (Lana-villarreal et al. 2010). The TiO_2 photoanodes were sensitized with CdS QDs using SILAR method(Santra and Kamat 2012). The photoanode is immersed for 1 min in 0.1 M ($Cd(NO_3)_2.4H_2O$) in methanol as a cation source (Cd^{+2}) and to be adsorbed on the TiO_2 electrode. The TiO_2 electrode was then rinsed with methanol to remove the excess Cd^{+2} cations. Then the photoanode is immersed in 0.1 M Na_2S methanolic solution as the anion source (S^{-2}) for 1 min in order to react with Cd^{+2} cations followed by methanol rinsing. This procedure was referred to as one

SILAR cycle. The SILAR cycles were repeated for 3, 4, 5 and 6 cycles. All the photoanodes were passivated by two SILAR cycles of ZnS as reported elsewhere (Zhu et al. 2011).

2. 3. Pt Counter Electrode Preparation

The platinum counter electrode was prepared through thermal decomposition of Chloroplatinic acid (H_2PtCl_6). A 20 µl of H_2PtCl_6 in isopropanol (5 mM) is spin coated on the previously cleaned FTO substrate of exposed area 1 cm^2 and then burned at 500 ^oC in air for 30 min. a transparent layer of Pt was formed on the FTO substrate to be used as a reference counter electrode in QDSSCs.

2. 4. Assembly Of Qdsscs

QDSSCs were constructing by assembling the TiO_2 photoanodes sensitized with CdS QDs and the counter electrodes into sandwich type solar cell using paper clamps as shown in figure (1). Parafilm was used as spacer between the two electrodes and also as a sealing to prevent the evaporation of the electrolyte. The space between the two electrodes was filled with aqueous polysulfide electrolyte. The polysulfide electrolyte prepared by dissolving 1M Na_2S, 1 M S, and 0.1 M KCl in deionized water.

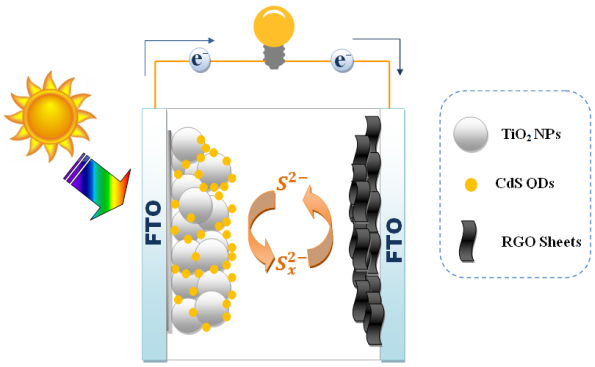

Fig. 1. Schematic representation of the assembled QDSSCs. The counter electrode was constructed by coating reduced graphene oxide RGO sheets on FTO substrate.

3. Results And Discussion

3. 1. Structural And Morphology Analysis

Figure (2) shows the UV- Visible absorption spectra of GO and the RGO. It is well known that pure GO has a strong absorption peak around 226 nm which belongs to the π→π* transition of C=C bond in GO. After the chemical reduction process, the absorption peak of GO is red shifted to 262 nm due to the completion of deoxygenation process. The absorption peak at 262 nm arise from the electrons n→π* transitions in addition to restoration of the electronic conjugation within the graphene upon hydrazine reduction (Ghadim et al. 2014; Khanra et al. 2012).

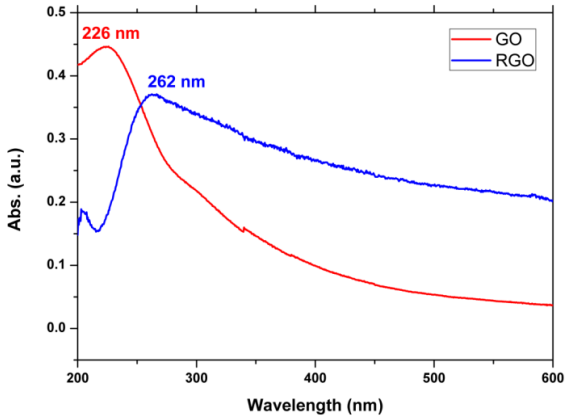

Fig. 2. UV-Visible absorbance spectra of GO and RGO.

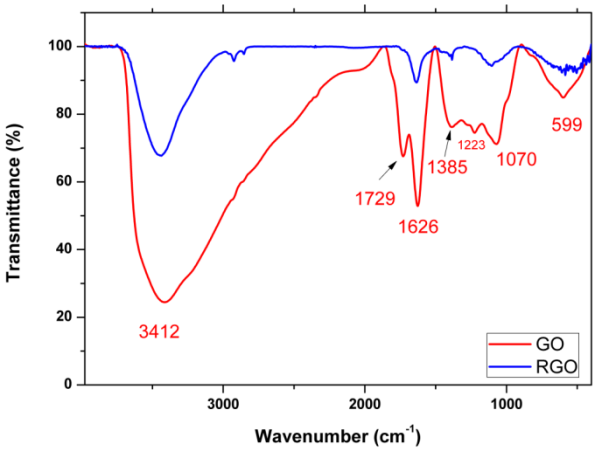

Fig. 3. FTIR spectra of the prepared GO and RGO.

To investigate the success of graphite oxidation process and the reduction process of graphene oxide, FTIR measurement was acquired. Figure (3) shows the FTIR spectra of GO and the chemically reduced graphene oxide (RGO). In GO spectrum, all the characteristic absorption peaks of carbon containing functional groups are present. The broad peak at 3412 cm^{-1} and the peak at 1385 cm^{-1} are due -OH stretching mode and bending deformation mode respectively, while the peak located at 1729 cm^{-1} is for C=O stretching in the carboxylic (-COOH) functional group located on GO sheets edges. The peaks at 1223 cm^{-1} and 1070 cm^{-1} are due to C-O stretching modes in the epoxy and alkoxy functional groups respectively. The strong peak at 1626 cm^{-1} is attributed to C=C in plane stretching for the unoxidized graphite (Yang et al. 2010; Zhang et al. 2010). In FTIR spectrum of RGO, the absorption peaks of -OH found in GO are significantly decreased in intensity, and the absorption peaks of C=O and C-O attributed to carbon containing groups are nearly disappeared. This observation implies that the deoxygenating process using hydrazine was performed successfully and sp^2 hybridization of graphene sheets was successfully restored.

The powder XRD was also employed as another characterization for the prepared GO and RGO as shown in Figure (4). In GO diffraction pattern, a clear and sharp characteristic peak of GO is located at 10.9º which corresponding to the (002) with inter-planer spacing (2d) of 8.14 Å. So the oxidation and functionalization processes of the graphite has been done and GO was successfully synthesized. After the reduction of GO, this peak was completely disappeared and a broad peak at 25.1º which is the characteristic peak of graphene was obtained. The new peak of the RGO is corresponding to 3.63 Å inter-planer spacing of graphene (Feng et al. 2013; Yang et al. 2010). Hence we can conclude that the success removal of the function groups, and a well ordered 2- dimensional graphene sheets was obtained.

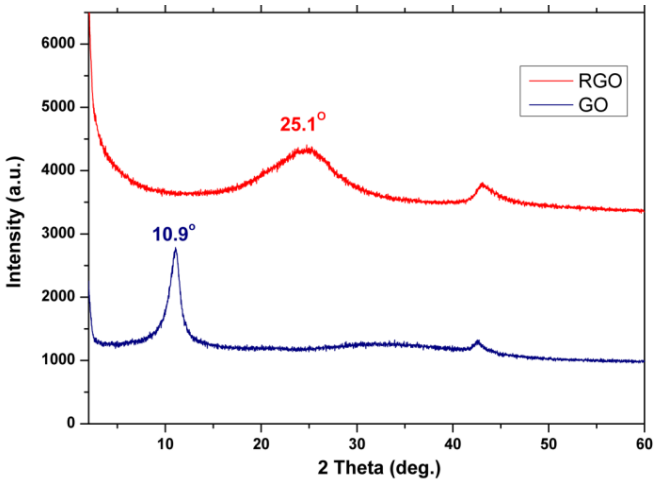

Fig. 4. X-ray diffraction patterns of the prepared GO and RGO.

The SEM micrographs of RGO counter electrode are shown in Figure (5). The well dispersed RGO sheets with homogeneous distribution of the sheets in the counter electrode can be seen clearly from the low magnification SEM micrograph. The high magnification micrograph confirms the 2-D layered structure of the few layers RGO sheets with wrapped edges resulting from using the PVDF as a binder. The wrapped edges of RGO sheets provides a high surface area of the counter electrode with more active sites which positively affecting the regeneration process of the electrolyte and it is reflected clearly in the high fill factor obtained when RGO used a counter electrode in QDSSCs.

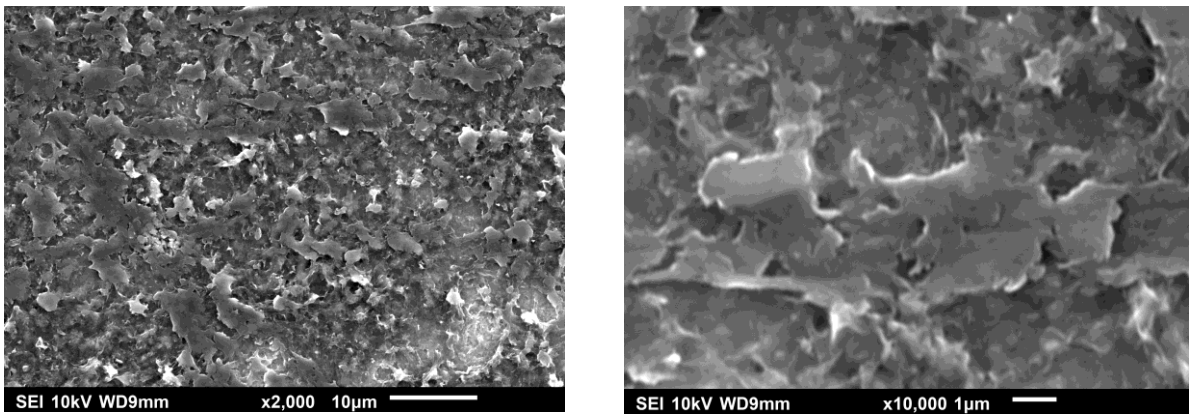

Fig. 5. SEM micrographs of RGO counter electrode (a) low magnification (b) high magnification.

3. 2. Electrochemical Characterization

The electrocatalytic activity of the prepared RGO and Pt counter electrodes towards polysulfide electrolyte was investigated using cyclic voltammetry (CV) and electrochemical impedance spectroscopy (EIS) techniques. Cyclic voltammograms of the prepared counter electrode was measured on a symmetrical cells composed of two identical counter electrodes (RGO\electrolyte\RGO or Pt\electrolyte\Pt). Ten cycles of CV was performed in the rage from -1 V to 1 V at a scan rate of 10 mV\sec and shown in Figure (6). Counter electrode made of RGO show higher stability in the presence of polysulfide electrolyte compared to CE made of Pt. the high stability of RGO was a result of the chemical inertness of graphene towards oxygen and water exist in the electrolyte (Choi et al. 2010). The reduction currents density of RGO CE are nearly constant around 13 mA\ cm^2 over the all ten cycles of CV, while that of Pt CE decrease with increasing the number of CV cycles to reach a value of 6 mA\ cm^2 at the end of the cycles. The decrease in the reduction current for Pt CE is mainly due to the poisoning of the platinum surface with sulfur components which reduces its electrical conductivity as well as its catalytic activity (Radich, Dwyer, and Kamat 2011). The relatively high catalytic activity of RGO CE can be attributed to the high electrical conductivity of RGO and the large surface area of the graphene which promote more active sites for the reduction process at the counter electrode. So, on the long term of QDSSCs running, RGO counter electrode with good electrocatalytic activity and high chemical stability will guarantee stable photovoltaic performance of the assembled solar cells.

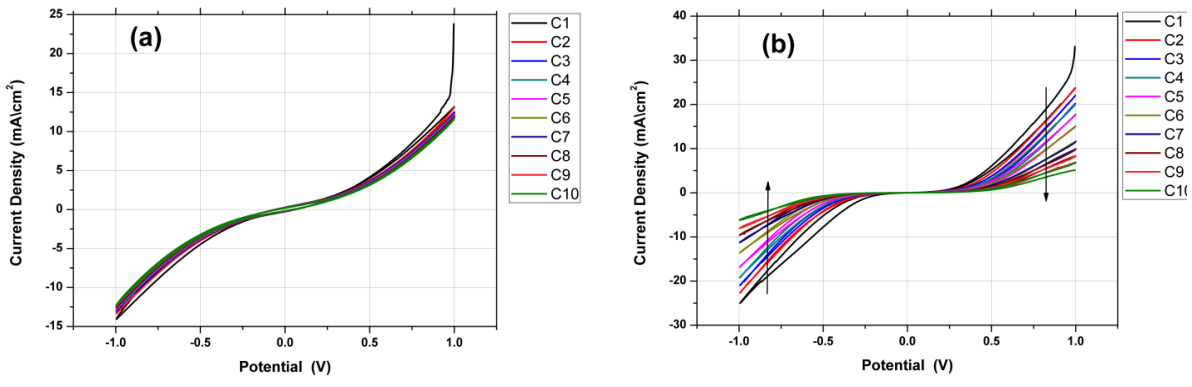

Fig. 6. cyclic voltammograms of symmetric cells composed of (a) RGO and (b) Pt counter electrodes acquired at scan rate 10 mV/s.

EIS measurements were performed on a dummy cell constructed from two symmetrical counter electrodes (RGO\electrolyte\RGO or Pt\electrolyte\Pt). The EIS test was performed within the frequency scan range from 10 mHz to 100 KHz with 10 mV RMS amplitude and 0 V DC bias voltage. The obtained EIS Nyquist plots of RGO and Pt counter electrodes are shown in Figure (7a). To extract the electrochemical parameters of the counter electrodes, the EIS data were fitted to the equivalent circuits indicated in Figure (7b) using ZsimWin software and the extracted data are listed in Table (1). As shown in Table 1, the series resistances (R_S) of the RGO and Pt counter electrodes are 17.3 and 16.5 Ω. cm^{-2} respectively, indicating that the bonding strength between RGO or Pt films on the underlying FTO substrate is high and comparable for both electrodes (Kim et al. 2014). The high bonding strength of RGO was arises from using PVDF polymer as a binder causing a good contact between the RGO sheets and FTO substrate. The charge transfer resistance (R_{CT}) for the RGO counter electrode is 55.9 Ω. cm^{-2}, which is one order of magnitude lower than that of the Pt counter electrode (558 Ω. cm^{-2}). The low R_{CT} of RGO counter electrode was a result of the high electron transfer rate occurs at RGO unlike that happens at the Pt electrode surface. These data are in consistent with CV measurements and indicates that the catalytic activity of the RGO counter electrode is better than the Pt towards the reduction of the polysulfide electrolyte. Probably, the high R_{CT} of Pt counter electrode arises from the surface poising of Pt by sulfur species.

Table. 1. The electrochemical parameters obtained from EIS data fitting.

	R_S (Ω)	R_{CT} (Ω.cm^{-2})	R_{Binder} (Ω.cm^{-2})
RGO CE	**17.3**	**55.9**	**165.4**
Pt CE	**16.5**	**558**	**—**

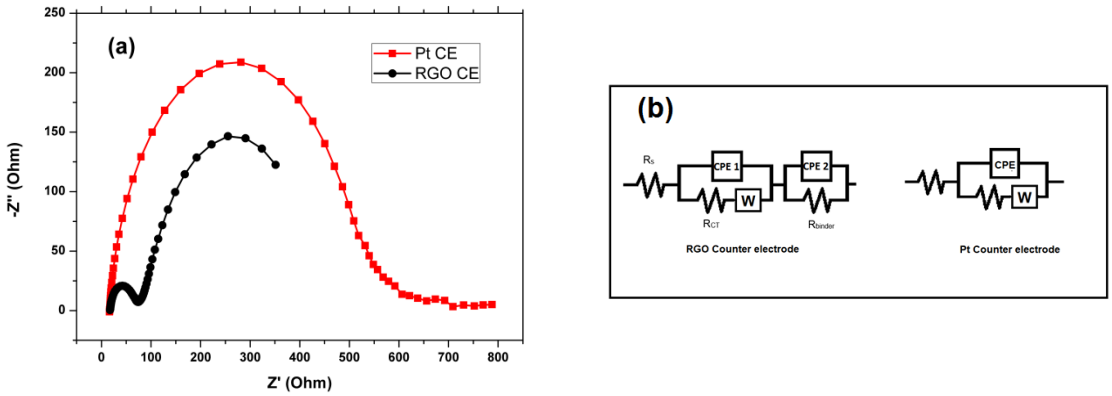

Fig. 7. (a) Nyquist plots of symmetric cells composed of RGO and Pt counter electrodes (b) Equivalent circuits for EIS data fitting.

3. 3. Photocurrent- Voltage Characterization

Photocurrent density – Photovoltage (J-V) curves of CdS QDSSCs based on RGO and Pt counter electrodes were characterized under standard simulated solar light of air mass coefficient (AM 1.5) and intensity of 100 mW/cm^2. The (J-V) curves of solar cells utilizing RGO counter electrode are presented in Figure (8), and the photovoltaic performance parameters are summarized in Table 2. The cell comprises TiO_2 photoanode sensitized with 3 CdS SILAR cycles shows the lowest PCE (0.12%), this because at this sensitization level the loading of CdS QDs was low. By increasing the number of the SILAR cycles, the PCE of the cells also increases due to the increase in the quantity of CdS QDs loaded on the TiO_2 mesoporous layer and more solar light is harvested. The PCE reaches a maximum value of (0.52%) for the cell assembled with TiO_2 photoannode sensitized by 5 SILAR cycles of CdS QDs and uses RGO as a counter electrode. The further increase in the SILAR cycles above 5 cycles causes a drop in the PCE and FF because at this level of sensitization the TiO_2 mesoporous is totally covered with CdS QDs and losing it porosity. This represents a barrier preventing the electrolyte to penetrate into the photoanode in order to reduce the deeply adsorbed oxidized QDs. It is worth

mentioned that, all QDSSCs assembled using RGO counter electrode had high FF and good short circuit current (J_{SC}). This behaviour can be attributed to the high electron transfer exist at the electrolyte \counter electrode interface arising from the high electric conductivity and large surface area of RGO counter electrode as was expected previously from the electrochemical measurements (Li et al. 2012).

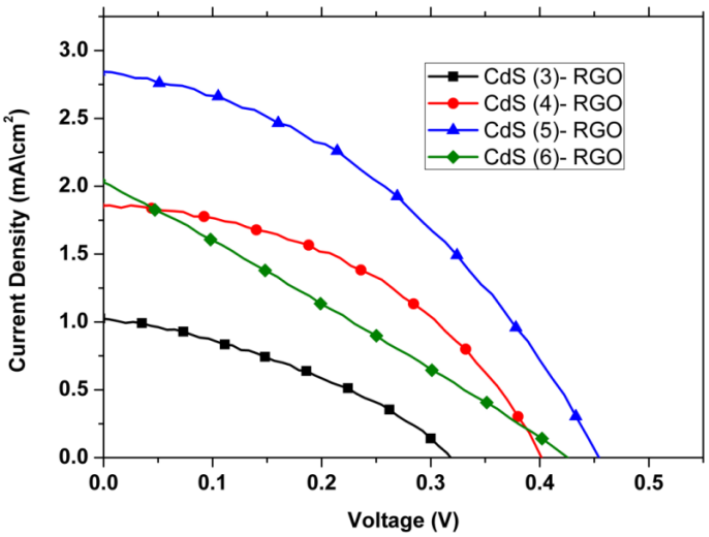

Fig. 8. Photocurrent density – Photovoltage (J-V) curves of QDSSCs sensitized with CdS QDs using SILAR method for 3 to 6 cycles and with RGO as counter electrode.

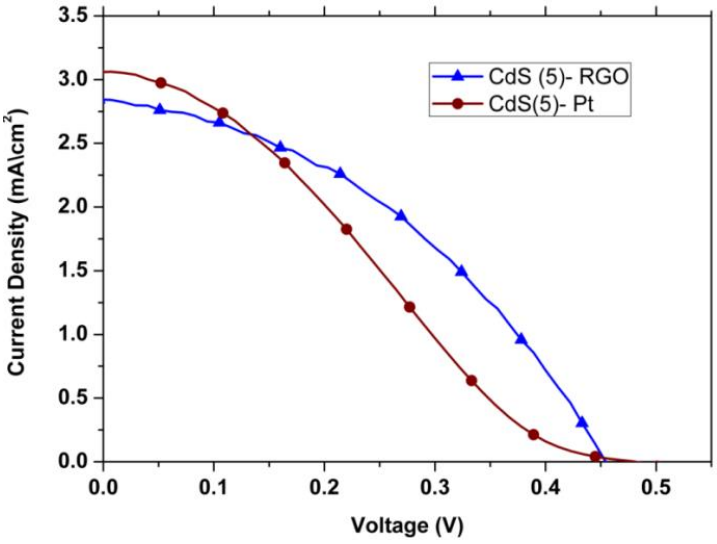

Fig. 9. Photocurrent density – Photovoltage (J-V) curves of QDSSCs sensitized with 5 SILAR cycles of CdS QDs when RGO or Pt used as counter electrode.

Figure (9) indicates a comparison between the (J-V) curves of two QDSSCs use RGO and Pt counter electrodes assembled with photoanode sensitized with 5 CdS SILAR cycles. Although the cell uses Pt shows Jsc of (3.06 mA\cm^2) higher than that use RGO counter electrode (2.84 mA\ cm^2), but the PCE of cell with RGO counter electrode was 30% higher than that use the Pt one. The reason for this manner was that, the fill factor of the cell with RGO counter electrode was 40.16% while that of the Pt was 27.4% , 31% lower than the RGO. So, counter electrode based on low cost, chemically stable, and good electrocatalytic activity RGO shows an enhancement in the photovoltaic performance of QDSSCs compared to the reference Pt counter electrode. For these reasons, graphene with proper design will be one of most suitable materials candidate to replace the incompatible and the expensive Pt counter electrode usually in QDs photo-electrochemical cells.

Table. 2. The Photovoltaic performance parameters of QDSSCs based on the different counter electrodes.

	V_{OC} (V)	J_{SC} (mA\cm^2)	FF %	PCE %
CdS (3)-RGO	0.318	1.022	36.49	0.12
CdS (4)-RGO	0.402	1.850	44.80	0.33
CdS (5)-RGO	0.455	2.843	40.16	0.52
CdS (6)-RGO	0.426	2.029	26.67	0.23
CdS (5)-Pt	0.481	3.059	27.45	0.40

4. Conclusion

RGO counter electrodes were successfully prepared by facile low temperature method and used in CdS QDSSCs. UV-visible, FTIR, and XRD analyses were employed to characterize the chemically prepared RGO. SEM was used to investigate the surface morphology of RGO counter electrode. The electrochemical activity and stability of RGO counter electrodes towards polysulfide electrolyte were checked using cyclic voltammetry CV and electrochemical impedance spectroscopy EIS. RGO counter electrode has been showed more electrochemical stability and activity than the Pt counter electrode as probed by CV. The charge transfer resistance (R_{CT}) extracted from EIS measurements of RGO counter electrode was one order of magnitude lower than that of the Pt. CdS QDSSCs used RGO as a counter electrode showed an enhancement 30% in PCE and 46.3% in FF than the cell that used Pt thin film counter electrode. The good electrical conductivity, the high chemical stability, and the large surface area of RGO were the key factors behind these enhancements in the photovoltaic performance of QDSSCs. our resulted data suggested that, graphene based materials may be the suitable materials to replace the lower active and expensive noble metals usually used as counter electrodes in QDSSCs.

Acknowledgements

The authors gratefully acknowledge the Missions Sector-Higher Education Ministry, Egypt for financial support through this work, and Materials Science and Engineering Department at E-JUST.

References

Badawi, A., Al-Hosiny, N., Abdallah, S., Negm, S., & Talaat, H. (2013). Tuning Photocurrent Response Through Size Control Of Cdte Quantum Dots Sensitized Solar Cells. *Solar Energy*, 88, 137–43. Retrieved September 5, 2014, from http://linkinghub.elsevier.com/retrieve/pii/S0038092X12003969.

Barceló, I., Campiña, J. M., Lana-Villarreal, T., & Gómez, R. (2012). A Solid-State Cdse Quantum Dot Sensitized Solar Cell Based On A Quaterthiophene As A Hole Transporting Material. *Physical chemistry chemical physics : PCCP*, 14(16), 5801–7. Retrieved June 2, 2014, from http://www.ncbi.nlm.nih.gov/pubmed/22426179.

Becerril, H. (2008). Evaluation Of Solution-Processed Reduced Graphene Oxide Films As Transparent Conductors. *ACS nano*, 2(3), 463–70. Retrieved from http://www.ncbi.nlm.nih.gov/pubmed/19206571.

Wonbong, C., Lahiri, I., Seelaboyina, R., & Kang, Y. S. (2010). Synthesis Of Graphene And Its Applications: A Review. *Critical Reviews in Solid State and Materials Sciences*, 35(1), 52–71. Retrieved July 14, 2014, from http://www.tandfonline.com/doi/abs/10.1080/10408430903505036.

Feng, H., Cheng, R., Zhao, Xin., Duan, X., & Li, J. (2013). A Low-Temperature Method To Produce Highly Reduced Graphene Oxide. *Nature communications*, 4, 1539. Retrieved August 5, 2014, from http://www.ncbi.nlm.nih.gov/pubmed/23443567.

Gamil, M. (2014). Graphene-Based Strain Gauge on a Flexible Substrate. 26(9), 699–709.

Geim, A. K., & Novoselov, K. S. (2007). The Rise Of Graphene. *Nature materials*, 6(3), 183–91. Retrieved July 11, 2014, from http://dx.doi.org/10.1038/nmat1849.

Ghadim, E. E. (2014). Pulsed Laser Irradiation For Environment Friendly Reduction Of Graphene Oxide Suspensions. *Applied Surface Science*, 301, 183–88. Retrieved August 6, 2014, from http://linkinghub.elsevier.com/retrieve/pii/S0169433214003201.

Hassan, S., Suzuki, M., & El-Moneim, A. A. (2014). Facile Synthesis Of Mno 2 / Graphene Electrode By Two-Steps Electrodeposition For Energy Storage Application. 9, 8340–54.

Kamat, P. V. (2008). Quantum Dot Solar Cells. Semiconductor Nanocrystals As Light Harvesters †. *The Journal of Physical Chemistry C*, 112(48), 18737–53. Retrieved March 26, 2014, from http://pubs.acs.org/doi/abs/10.1021/jp806791s.

Khanra, P. (2012). Simultaneous Bio-Functionalization And Reduction Of Graphene Oxide By Baker's Yeast. *Chemical Engineering Journal*, 183, 526–33. Retrieved August 8, 2014, from http://linkinghub.elsevier.com/retrieve/pii/S1385894711016263.

Kim, H.-J. (2014). Improved Performance Of Quantum Dot-Sensitized Solar Cells Adopting A Highly Ef Fi Cient Cobalt Sul Fi De / Nickel Sul Fi De Composite Thin Fi Lm Counter Electrode. 268, 163–70.

Kouhnavard, M. (2014). A Review Of Semiconductor Materials As Sensitizers For Quantum Dot-Sensitized Solar Cells. *Renewable and Sustainable Energy Reviews*, 37, 397–407. Retrieved August 6, 2014, from http://linkinghub.elsevier.com/retrieve/pii/S1364032114003487.

Kucinskis, G., Bajars, G., & Kleperis, J. 2013. Graphene In Lithium Ion Battery Cathode Materials: A Review. *Journal of Power Sources*, 240, 66–79. Retrieved January 27, 2015, from http://linkinghub.elsevier.com/retrieve/pii/S0378775313005545.

Lana-Villarreal, T., Shen, Q., Toyoda, T., & Go, R. (2010). Sensitization of Titanium Dioxide Photoanodes with Cadmium Selenide Quantum Dots Prepared by SILAR : Photoelectrochemical and Carrier Dynamics Studies Ne. 3, 21928–37.

Li, Z.-Y., Akhtar, M. S., Kuk, J. H., Kong, B.-S., & Yang, O. B. (2012). Graphene Application As A Counter Electrode Material For Dye-Sensitized Solar Cell. *Materials Letters*, 86, 96–99. Retrieved December 16, 2014, from http://linkinghub.elsevier.com/retrieve/pii/S0167577X12009664.

O'Regan, B., & Grätzel, M. (1991). A Low-Cost, High-Efficiency Solar Cell Based On Dye-Sensitized Colloidal Tio2 Films. *Nature*, 353(6346), 737–40. Retrieved July 14, 2014, from http://dx.doi.org/10.1038/353737a0.

Pei, S., & Cheng, H.-M. (2012). The Reduction Of Graphene Oxide. *Carbon*, 50(9), 3210–28. Retrieved July 10, 2014, from http://linkinghub.elsevier.com/retrieve/pii/S0008622311008967.

Radich, J. G., Dwyer, R., & Kamat, P.V. (2011). Cu 2 S Reduced Graphene Oxide Composite for High-Efficiency Quantum Dot Solar Cells. *Overcoming the Redox Limitations of S 2*. 2453–60.

Rühle, S., Shalom, M., & Zaban, A. (2010). Quantum-Dot-Sensitized Solar Cells. *Chemphyschem : a European journal of chemical physics and physical chemistry*, 11(11), 2290–2304. Retrieved April 4, 2014, from http://www.ncbi.nlm.nih.gov/pubmed/20632355.

Santra, P. K., & Kamat, P.V. (2012). Mn-Doped Quantum Dot Sensitized Solar Cells: A Strategy To Boost Efficiency Over 5%. *Journal of the American Chemical Society*, 134(5), 2508–11. Retrieved from http://www.ncbi.nlm.nih.gov/pubmed/22280479.

Strong, V. (2012). Patterning and Electronic Tuning of Laser Scribed Graphene for Flexible All-Carbon Devices. 2, 1395–1403.

Sui, D. (2011). Flexible And Transparent Electrothermal Film Heaters Based On Graphene Materials. *Small*, 7(22), 3186–92. Retrieved November 19, 2013, from http://www.ncbi.nlm.nih.gov/pubmed/21990210.

Yang, N., Zhai, J., Wang, D., Chen, Y., & Jiang, Lei. (2010). Two-Dimensional Graphene Bridges Enhanced Photoinduced Charge Transport In Dye-Sensitized Solar Cells. *ACS Nano*, 4(2), 887–94. Retrieved from http://www.ncbi.nlm.nih.gov/pubmed/20088539.

Zhang, J. (2010). Reduction Of Graphene Oxide Via L-Ascorbic Acid. *Chemical Communications*, 46(7), 1112–14. Retrieved July 9, 2014, from http://www.ncbi.nlm.nih.gov/pubmed/20126730.

Zhu, G. (2011). Graphene-Incorporated Nanocrystalline Tio2 Films For Cds Quantum Dot-Sensitized Solar Cells. *Journal of Electroanalytical Chemistry*, 650(2), 248–51. Retrieved April 10, 2014, from http://linkinghub.elsevier.com/retrieve/pii/S1572665710004091.